J Solid State Electrochem (2010) 14:1985–1995
DOI 10.1007/s10008-010-1036-6

ORIGINAL PAPER

Polypyrrole on self-assembled monolayers of a pyrrolyl lipoic acid derivative—electrosynthesis and polymer film characterization

Ana Mourato · Ana S. Viana · Franz-Peter Montforts · Luisa Maria Abrantes

Received: 16 December 2009 / Revised: 18 February 2010 / Accepted: 21 February 2010 / Published online: 25 March 2010

Abstract The electropolymerization of pyrrole on gold modified by a self-assembled monolayer (SAM) of a pyrrolyl lipoic acid derivative was investigated in detail and the results compared to those obtained on bare substrates. Both under potentiostatic and potentiodynamic control, a slight blocking action of the underlying SAM could be observed for the initial stages of polymer growth but thereafter the electrochemical features were similar to those collected for polypyrrole (PPy) deposition on bare gold. The morphology and structure of PPy films formed on the SAMs were characterized by atomic force microscopy and X-ray diffraction, which revealed that those polymer properties are much more influenced by the electrochemical mode of preparation, than by the underlying SAMs. While, when compared to PPy on bare gold, no effect has been detected on thin layers deposited at constant potential, surface areas with rather irregular morphology, as well as a small but beneficial influence in inducing order on the first few layers of the polymer film, have been observed on similar films formed by cyclic voltammetry. The typical globular morphology of PPy has always been observed for relatively thick layers in which the redox behavior, analyzed by in situ AFM, showed an increase in volume of the polymer nodules upon reduction, largely due to the SAM reorganization induced by the applied potential.

Keywords Electropolymerization · Polypyrrole · Functionalized self-assembled monolayers · Polymer structure · Morphology

A. Mourato · A. S. Viana · L. M. Abrantes (✉)
CQB, Departamento de Química e Bioquímica,
Faculdade de Ciências da Universidade de Lisboa,
Campo Grande,
1749-016 Lisbon, Portugal
e-mail: luisa.abrantes@fc.ul.pt

F.-P. Montforts
Institut für Organische Chemie,
FB 2 Biologie/Chemie der Universität Bremen,
Postfach 330 440,
Bremen 28334, Germany

Introduction

Electrochemical deposition of conducting polymers has been studied extensively. A pursuit in some recent investigations is the improvement of several characteristics of the generated polymer films, to make them attractive candidates for new applications such as organic electronics and nanotechnology. It is known that the surface properties of the substrate where the polymer is deposited control the polymerization process as well as the order, crystallinity, morphology, and adherence of the films [1–6].

One of the most employed strategies to modify the substrate surface, altering either the properties of the film (improving mechanical and electrochemical stability [7]) or the electrochemical deposition (avoiding the adhesion, patterned deposition [8]), is the use of surface-confined monomers; this can be achieved through electrochemical grafting [9], Langmuir–Blodgett technique [10] or self-assembly [11]. In spite of the formation of strong chemical bonds assured by the grafting approach [9, 12, 13], e.g. electrochemical reductive adsorption of functionalized aryl diazonium salts, this method does not grant a strict control over the number of layers (mono/multilayers), and thus on the molecular arrangement on the electrode surface. Self-assembled monolayer interfaces can be used to change the surface energy and/or to provide nucleation sites for covalent grafting of the polymer chains [14–16]. Although

self-assembly is a random process [17] rendering impossible to access the amount of defects in the monolayer, the integrity of SAMs films prepared with compounds bearing terminal monomer functionality appears to be satisfactory and such interfaces have been reported as efficient not only to assure the order of the confined monomers [18] but also to induce good crystallinity at the substrate–polymer interface [19–23].

It is well known that using thiol-based compounds high-quality monolayers are formed on gold electrodes [24]. Although there are numerous reports on the electrochemical behavior of monomer-terminated monolayers on gold electrodes [25, 26], only a few papers are devoted to other substrates [18, 27].

Pyrrole-containing alkanethiol monolayers have been adhesion promoters molecules of choice to increase the polypyrrole (PPy) film adhesion on Au surfaces, as a result of the high interaction Au–S and of the low potential value for pyrrole oxidation, enabling the polymerization process well before the thiol oxidative desorption would take place [4, 28–37].

It is generally accepted that monolayers containing pyrrolyl groups enhance the nucleation and growth of PPy conducting films electrodeposited from pyrrole-containing solutions [11, 32, 34, 38–44]. Willicut et al. in 1995 [11, 40] concluded that an enhancement of the nucleation, growth, smoothness, and adhesion of PPy films was obtained by using gold modified by short chain of ω-(*N*-pyrrolyl) alkanethiol molecules. Collard et al. [39] have also shown that w-(3-pyrrolyl) alkanethiols with long alkyl chains form well-ordered monolayers and by electrodeposition of 3-ethyl pyrrole, an electroactive, smooth, and adherent polymer film is obtained. The epitaxial growth of *N*-hexadecylpyrrole was achieved by electrochemical deposition on monolayers of (w-(*N*-pyrrolyl)-*n*-undecyl disulfide) on gold surfaces [1, 31]. It was found that at potentials sufficiently positive to oxidize *N*-hexadecylpyrrole, the surface-confined pyrroles form radical cations, which establish a covalent bond, by coupling reaction, with the monomer radical cations, thus acting as nucleation sites. Worth mentioning, that most of all these studies were carried out in organic media; less attention has been paid to aqueous electrolytes.

On other substrates, studies focusing both the electropolymerization of surface-confined monomers and the effect of such interfaces on polymer deposition and film properties [18, 23, 45–48] have been mainly devoted to polyaniline. Using silicon substrates modified with self-assembled amino-silane monolayer, the growth of a highly crystalline polyaniline film at the polymer–substrate interface has been observed [23] which provides evidence on the important role of substrate surface in determining the structure and morphology of the deposited polymer; also, the electrochemical deposition of aniline on indium tin oxide (ITO) modified with an aniline-terminated silane derivative, showed that polymer deposition rates decrease, and polymer films display smaller grains than when prepared on unmodified ITO [18].

In this work, a specially synthesized lipoic acid pyrrolyl derivative is used to modify the electrode surface, granting an efficient bidding to gold, by self-assembly throughout the two sulfur atoms, as recently reported in a paper devoted to the formation and electrochemical behavior of such SAMs [49]. The electrodeposition of PPy films on the modified gold electrodes is investigated in detail; the influence of the SAM on the polymer nucleation and growth is analyzed and contrasted to the responses of PPy films electrosynthesized on bare gold. The morphological and structural properties of thin and thick layers are addressed by atomic force microscopy (AFM) and X-ray diffraction (XRD).

Experimental

The synthesis of the 3-(1H-pyrrol-1-yl)propyl 5-[(3R)-1,2-dithiolane-3-yl] pentanoate (Py-LA; Scheme 1) has been reported elsewhere [49]. The monomer pyrrole (Py—Sigma-Aldrich) was purified by distillation under reduced pressure, prior to use. The lithium perchlorate ($LiClO_4$—Fluka, purity ≥99%) was recrystallized with ethanol. All aqueous solutions were prepared with Millipore-Q water (nominal resistivity of 18 MΩ at 25 °C).

The electrochemical measurements were performed using a set of equipments consisting on a potentiostat (Wenking LB 75L), a voltage scan generator (Wenking VS683), a double pulse control generator (Wenking DPC 72) and a Recorder X-Y Model 2000 (The Recorder Company).

Two different Au-working electrodes were used: gold slides (Gold Arrandee, GmbH) (with an exposed area of 0.48 cm^2) and free gold polycrystalline disks (99.99%, area 0.5 cm^2). For each experiment, the gold slides substrates were cleaned with *piranha* solution, washed with ethanol and water and dried with N_2 (purity >99.99997%) flow.

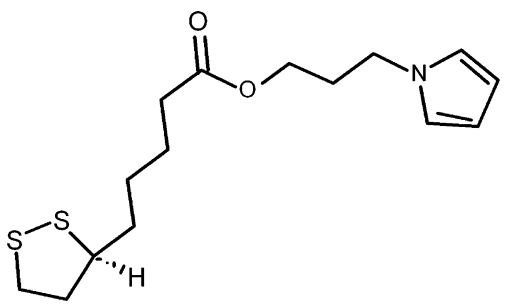

Scheme 1 3-(1H-pyrrol-1-yl)propyl 5-[(3R)-1,2-dithiolane-3-yl] pentanoate (Py-LA)

This procedure was followed by flame-annealing, to produce a flat surface with a predominant (1 1 1) crystallographic orientation. For the gold-free disks a fresh mirror-finish surface was generated by hand-polishing the electrode in an aqueous suspension of successively finer grades of alumina (down to 0.05 μm). A Pt foil (1 cm^2) and a saturated calomel electrode (SCE) were employed as counter electrode and reference electrode, respectively. For the studies using the gold slides, a one-compartment Teflon cell was used, whereas a three-compartment cell was employed for the experiments with the gold disk.

Deposition of monolayers of pyrrole-containing lipoic acid derivatives was achieved by immersing the gold slides in 1 mM Py-LA ethanolic solution, during 16 h. The PPy electropolymerization was performed on Au (111), polycrystalline Au and Au (111)/Py-LA SAM electrodes, from an aqueous solution of 0.1 M LiClO4, containing 0.03 M pyrrole, under potentiodynamic and potentiostatic modes. The films synthesized potentiodynamically were obtained by cycling the potential between −0.600 and +0.740 V at a sweep rate of 0.05 V s^{-1}, whereas for the potentiostically grown films the potential was stepped from the open circuit potential to +0.700, +0.740, +0.792 or +0.882 V vs. SCE. The same aqueous electrolytic solutions were used to characterize the modified electrodes, by CV in the potential range of −0.400 to +0.400 V at 0.05 Vs^{-1}. All the solutions were deoxygenated directly in the electrochemical cell with a stream of N_2 for at least 20 min prior to each experiment and the measurements were carried out at room temperature.

The structural characterization of the so-obtained PPy films was done by X-ray powder diffraction in a Philips X-ray diffractometer (PW 1730) with automatic data acquisition (APD Philips v3.6B) using Cu K_α radiation (λ= 0.15406 nm) and working at 30 kV/40 mA. The X-ray patterns were obtained in the 2θ range of 2° to 30°, using a 0.005° step size. The morphology of the modified electrodes was examined with a Nanoscope IIIa Multimode Atomic Force Microscope (Digital Instruments, Veeco) at room temperature. In situ experiments were performed using a commercial electrochemical AFM (ECAFM) cell (Digital Instruments, Veeco), containing platinum wires as counter and pseudo-reference electrodes. The platinum wires were flame-annealed before each experiment. The stability of the pseudo-reference electrode in the ECAFM cell was routinely checked, and the voltammograms obtained were compared to the ones recorded in a conventional electrochemical cell with a saturated calomel electrode. Therefore, all potentials cited in this paper have been converted to SCE. The ex situ AFM images were obtained in tapping mode, using etched silicon tips (resonance frequency of ca. 300 kHz), whereas the in situ measurements were performed in contact mode, using V-shape silicon nitrite cantilevers.

Results and discussion

The voltammetric response of the monolayer-modified electrodes bearing one pyrrole group (Py-LA SAM), in 0.1 M LiClO4 aqueous solution, is illustrated in Fig. 1. The irreversible oxidative wave, centered at about 0.9 V (oxidation peak I), corresponds to the oxidation of the pyrrole terminal groups since it is absent in gold electrode coated with octyl-LA monolayers; as shown in a previous paper [49] the monolayers resists to this electroxidation step: after oxidation of the surface-confined monolayer (10 cycles between 0 and 1.0 V) no changes in the SAM blocking properties toward a solution redox probe, $K_3Fe(CN)_6$, were observed. However, sweeping the potential to further positive values, the oxidative desorption of the monolayers from gold (oxidation peak II) occurs and the reverse potential sweep disclose the characteristics of the bare gold electrode (reduction peak III and IV). Peak II is sharp and displays high current for Py-LA SAM which might be explained by an intrinsic structural organization and by the contribution of the change in ion pairing upon oxidation of the pyrrole moieties. The presence of a large background current at high positive potentials, prevents a direct evaluation of the surface coverage from the charge beneath that oxidation peak; considering a second potential cycle as an appropriate background current, and the transfer of six electrons associated with the oxidative desorption of the dithiolane moiety, the estimated surface coverage is 5.2×10^{-10}mol cm^{-2}. This value, is in reasonable agreement with those obtained for the electrochemical reductive desorption [49], and with the effect of the size of the end group when compared to octyl-LA SAMs or close-packed *n*-alkanethiols SAMs on gold substrates [50–52].

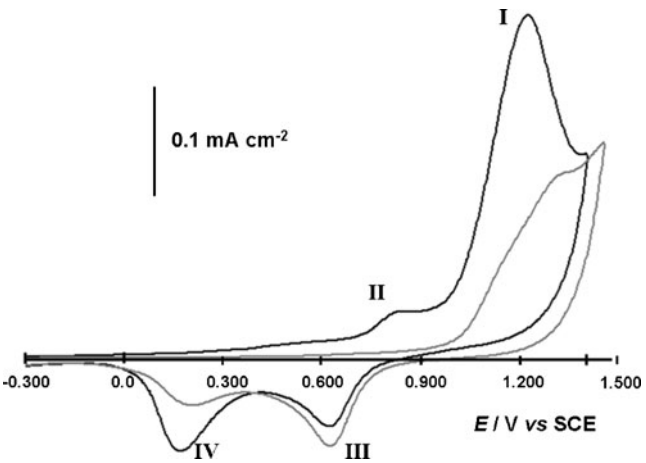

Fig. 1 Electrochemical oxidative desorption of pristine Octyl-LA (*light gray*) and Py-LA SAMs (*dark gray*) from Au substrate; 1 h of deoxygenation, in 0.1 M $LiClO_4$; ν=0.05 V s^{-1}

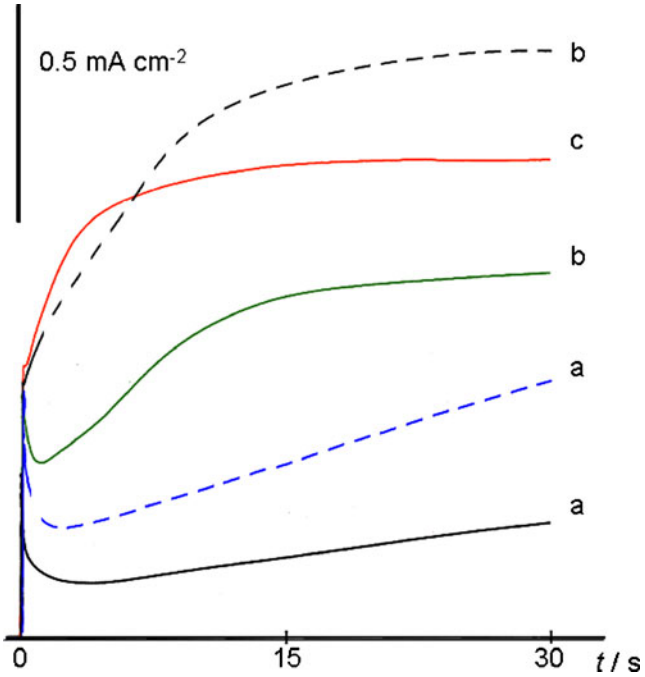

Fig. 2 Current–time transients recorded during the potentiostatic growth of PPy on Au polycrystalline (*dashed line*) and Au (111) slide (*solid line*) electrode. The potential steps were applied from the open circuit potential (≈0.00 V vs. SCE) to the growth potential (E_g) **a** E_g= 0.700 V, **b** E_g=0.792 V, and **c** E_g=0.882 V, in an electrolyte solution of 0.03 M Py in 0.5 M $LiClO_4$

The electropolymerization of Py, from solutions containing 0.03 M Py in 0.1 M $LiClO_4$, was performed at potentials bellow 0.95 V, to assure the integrity of the SAMs.

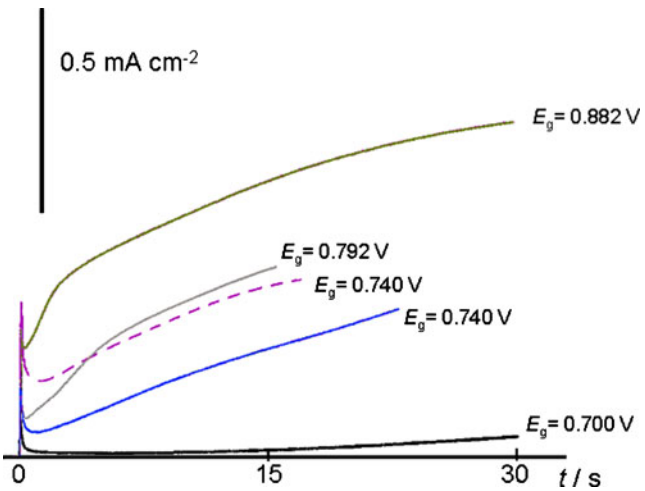

Fig. 3 Current–time transients recorded during the potentiostatic growth of PPy on Au (111)/Py-LA SAM (*solid lines*). The potential steps were applied from the open circuit potential (≈0.05 V vs. SCE) to E_g=0.700 V, E_g=0.740 V, E_g=0.792 V, and E_g=0.882 V, in an electrolyte solution of 0.03 M Py in 0.5 M $LiClO_4$. *Dashed line* corresponds to current–time transient recorded during the potentiostatic growth of PPy on Au (111) at E_g=0.740 V

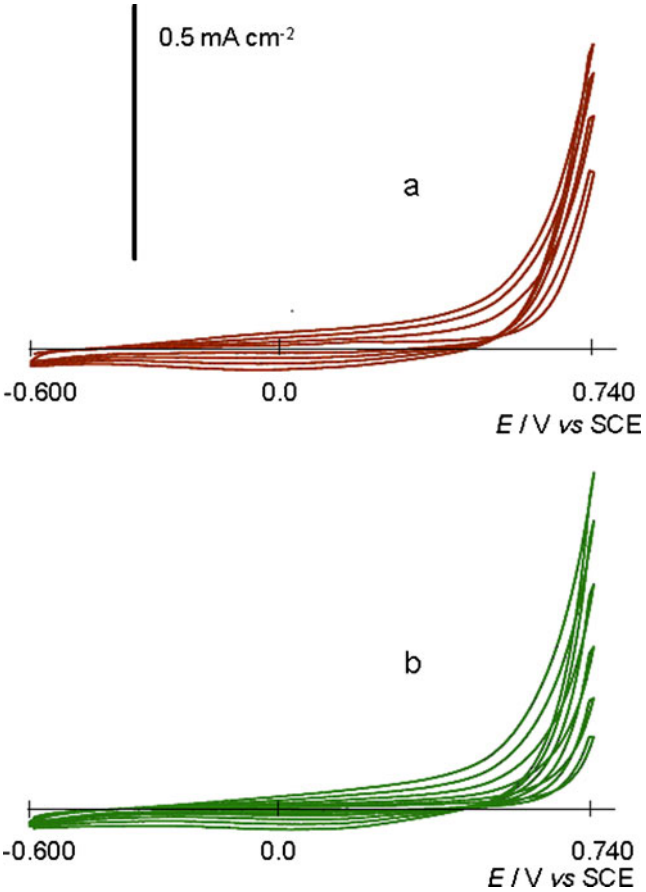

Fig. 4 Cyclic voltammograms of the electropolymerization of polypyrrole from 0.03 M Py in 0.5 M $LiClO_4$ at ν=0.05 Vs^{-1} on **a** Au (111) slide electrode (four cycles) and **b** Au (111)/Py-LA SAM (six cycles)

For a series of applied potentials, typical current transients [53] were observed for the potentiostatic polymerization of Py on polycrystalline gold and on the slides modified with Py-LA SAM (Fig. 2). Stepping the potential from an initial value where no electron transfer occurs, e.g. the open circuit potential, to a value where the oxidation takes place, at t=0 the double-layer charging originates the current spike, which decays exponentially with time and is superimposed by the Faradaic current from the electrochemical reaction; the evolved time to reach the lowest current density value in the transient, indicative of the nucleation process onset, decreases as the growth potential

Fig. 5 AFM-tapping mode images of a PPy films grown potentiodynamically (10 polymerization cycles at ν=0.05 Vs^{-1}) on Py-LA SAM (**a**) and Au (111) slide electrode (**b**), comparison between AFM height and phase contrast images (**c**); 1×1 μm^2 window size, detail (0.5× 0.5 μm^2) of image a-right (**d**), and polymer formed with on 25 polymerization cycles at ν=0.05 Vs^{-1} on Py-LA SAM (**e**): left image 2×2 μm^2 and right image with 1×1 μm^2 window size. Z scale equal to 30 nm for 3D-processed topographic top image (**a**), 40 nm for the other three images in (**a**), (**b**), (**c**) and right image in (**e**)

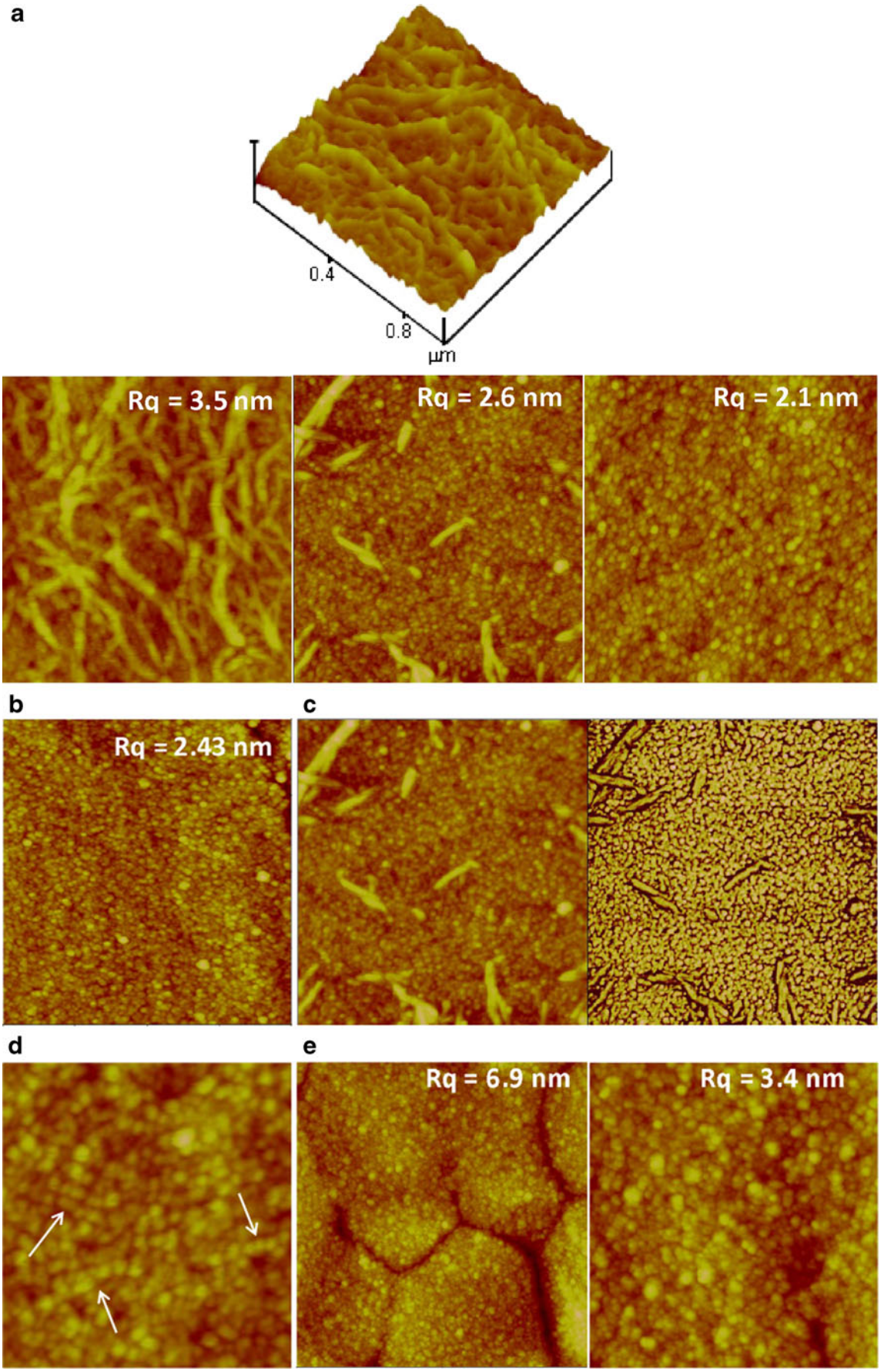
a
0.4
0.8
µm
Rq = 3.5 nm
Rq = 2.6 nm
Rq = 2.1 nm
b
Rq = 2.43 nm
c
d
e
Rq = 6.9 nm
Rq = 3.4 nm

increases. This process is much clearly observed for the PPy films deposited on gold (111) surface than on polycrystalline gold, as illustrated respectively by the distinct profiles of solid and dashed b curves in Fig. 2. Therefore, smooth gold (111) was chosen to investigate the influence of the underlying SAM onto PPy electrochemical deposition. Also, a predominant crystallographic orientation enables a better organization and packing of the monolayer.

The effect of the Py-LA SAM on the nucleation and growth of PPy can be observed in Fig. 3. Although all stages involved in the polymer deposition develop at lower rate than on bare gold no significant blocking effect due to the presence of the monolayer can be retrieved. The oxidation of the pyrrolyl terminal groups, to form radical cations necessary for polymerization, prior to the oxidation of pyrrole from solution and the coupling of surface-confined species to monomer/radical cations from solution, leading to a covalent bond between the monolayer and the deposited film, might explain the experiential differences in the current transients [7, 11, 32, 34, 39–44].

By virtue of a high number of available nucleation sites on the modified surfaces, it is expected that the polymer deposition exhibits an enhanced nucleation [1]. Indeed, that appears to be the case for Py-LA SAM where the monolayer discharge and nucleation onset occurs at shorter time than on bare gold. Also, the augment in current during polymerization points to an increasing electroactive surface area.

The potentiodynamic deposition of PPy onto bare and modified gold electrodes is shown in Fig. 4a and b, respectively. The characteristic features, e.g. monomer oxidation and progressive increase of the waves assigned to PPy redox conversion, can be clearly seen, but the respective current responses are again higher for polymer deposition on bare gold than on the SAM-modified electrode.

The first few layers between the base electrode and the further deposited polymer are very important for the adhesion and in developing the morphology and structure of thicker polymer films. The PPy films deposited on Py-LA SAM, with a relatively low number of potential cycles, i.e. well before the film starts to increase its thickness substantially, display an irregular morphology where areas with long segments can be observed (Fig. 5a), dissimilarly to the typical regular globules observed for PPy films deposited on gold (Fig. 5b). A comparison between the AFM height image and the one obtained by phase contrast analysis, very sensitive to changes in the composition of the surface, Fig. 5c, advocate that the nodules and the segments have the same composition and thus are made of the same material.

As reported previously [49], scanning tunneling microscope (STM) imaging of Py-LA SAM electrodes after being submitted to oxidation, in the absence of Py in solution, reveal the formation of aggregates; these might be responsible for the observed morphology of the first layers of the deposited PPy. Indeed, looking in detail at the AFM image, some organization in the globular region can also be observed as pointed by the arrows in Fig. 5d. Nonetheless, typical globular morphology is observed for thick (25 potential cycles) PPy films (Fig. 5e).

As expected from the features of the current transients, the morphology of thin PPy films prepared at constant potential is also affected by the underlying SAM. It is very likely that the preceding oxidation of the terminal groups of the SAM and so-formed agglomerates act as seeds, promoting the instantaneous nucleation of the nascent polymer film, originating grains on its top as divulged in Fig. 6.

One of the main aims in using substrates modified by SAMs bearing a Py terminal functionality for the electropolymerization of Py from solution is the development of ordered structures which are known to contribute for the enhancement of the conductivity of the growing film [54, 55]. A direct relationship between the synthesis conditions and the final structure is hard to achieve since most of the structural information is obtained ex situ, thus after submitting the films to washing and drying treatments. Nevertheless, based on X-ray diffraction patterns, it has been reported in the literature that PPy presents a large

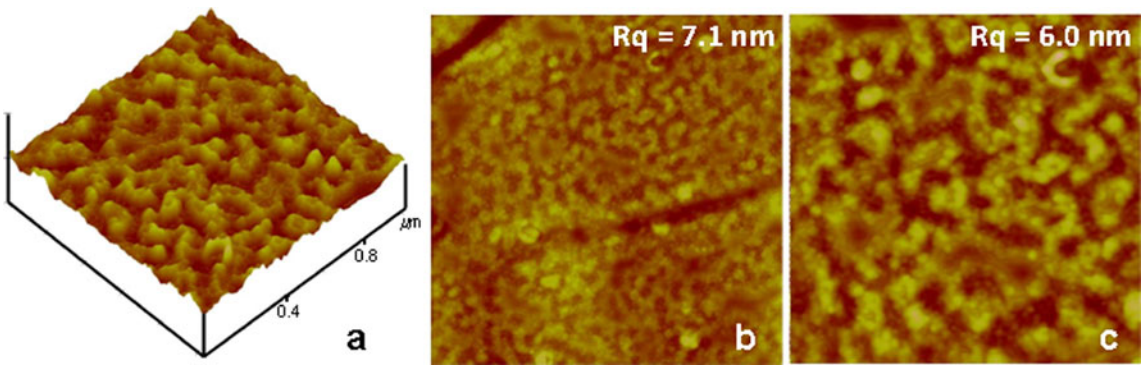

Fig. 6 AFM-tapping mode topographic images of PPy films grown potentiostatically at E_g=0.740 V on Au (111)/Py-LA SAM, (**a**) 3D representation, *Z*=60 nm (1×1 μm^2); (**b**) 2×2 μm^2 and (**c**) 1×1 μm^2 window sizes, for both images *Z*=40 nm

amount of disorder, being the X-ray peaks broad Gaussians [56, 57]. The main peak, occurring at about 2θ=19°, has been attributed to the amorphous regions of the polymer [57–59]. A crystal peak at 2θ≈5° and, when the polymer growth is conducted at very low rates, semicrystalline regions showing peaks at about 2θ=13°, assigned to the characteristic interchain repeat unit and in the region 2θ=22 to 27°, related to the pi-stacked rings of PPy, have also been described [56, 58, 59].

To examine the effect of the underlying SAM on the structural properties of the deposited PPy, thin films were potentiodynamically prepared on bare and modified gold; four and six potential scans were used respectively, in order to observe films displaying similar electroactivities (oxidation charge, Q_{ox}≈0.5 mC cm^{-2}). The X-ray diffractograms are presented in Fig. 7. The spectrum obtained from the layer on Au is typical of those reported for PPy, i.e. a very broad peak centered at 2θ=18°, denoting the amorphous nature of the polymer. In the case of PPy grown on the SAM, this peak suffers a significant decrease in intensity and is followed by another slightly higher and sharper at 2θ≈22°, suggesting that the SAM has a beneficial effect, even small, in inducing order on the first few layers of the polymer film, probably due to a contribution of two effects: an increase in the number of nucleation sites and to the SAM reorganization induced by the potential cycling [60].

The X-ray diffraction patterns of the set of films, prepared potentiostatically, are depicted in Fig. 8. In contrast to the data shown in Fig. 7, reflected intensities are found between 12° and 26°, pointing to the presence of semicrystalline PPy (small but sharp peaks at 2θ=12.5° and 25° and two not completely resolved peaks in the region around 20°). These remarkable differences are undoubtedly attributable to the electrochemical mode and conditions employed to grow the polymer. Moreover, it is clearly noticeable that there is no influence of the underlying SAM in the structure of the polymer films potentiostatically deposited.

Certain systematic changes can be observed in the diffractograms of Fig. 8. An augment of about 0.050 V in the growth potential (from 0.740 to 0.782 V), either using bare or modified gold, results in a poorer crystallinity of PPy, denoted by the decrease in intensity of all peaks and by the less resolution of those around 2θ=20°. A lower crystalline character is also perceived for thicker films; a non-negligible reduction in peaks intensity is detected for PPy grown with 12 mC cm^{-2}, when compared to a film prepared with 5 mC cm^{-2}. These observations agree with previous reports, namely supported on AFM experiments, revealing highly orientated growth nuclei of PPy deposited at constant potential, over a gold electrode [61], and based on ex situ X-ray experiments, showing that the first layers of PPy films are flat and orientated whilst additional overlayers are oriented randomly [62].

The voltammetric responses of the PPy films prepared under the described conditions, in fresh monomer-free electrolyte, allow to compare the polymer redox behavior. In early days, the charge compensation accompanying the

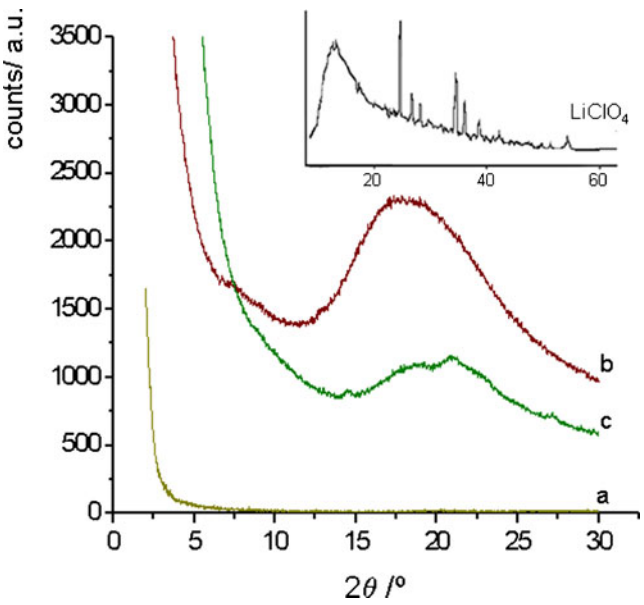

Fig. 7 XRD patterns of Au (111) slide electrode (**a**) and PPy films electropolymerized onto Au(111) with four cycles (**b**) and on Au(111)/Py-LA SAM with six cycles (**c**), in 0.03 M Py+0.1 $LiClO_4$ at υ=0.05 V s^{-1}. *Inset* XRD patterns of the supporting electrolyte, $LiClO_4$ [75]

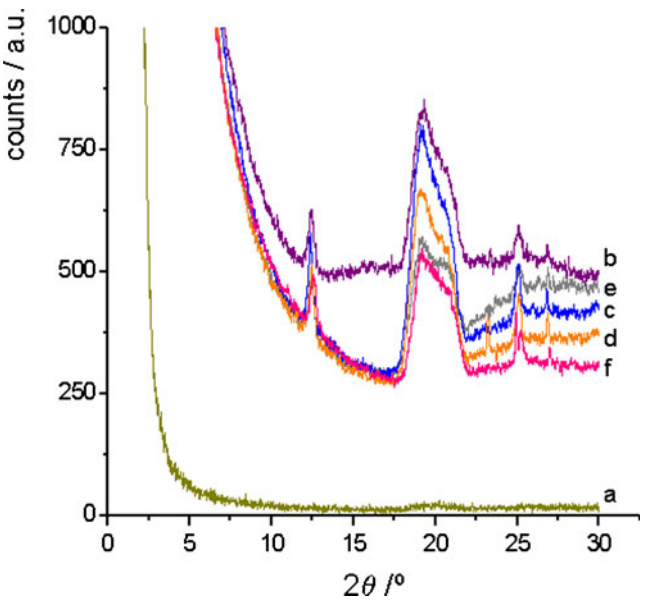

Fig. 8 XRD patterns of **a** Au (111) slide electrode and PPy films grown potentiostatically in 0.03 M Py+0.1 $LiClO_4$, **b** Au(111)/PPy: E_g=0.740 V, growth charge (Q_g)=5.8 mC cm^{-2}, **c** Au (111)/Py-LA SAM/PPy: E_g=0.740 V, Q_g=5 mC cm^{-2}, **d** Au (111)/Py-LA SAM/PPy: E_g=0.740 V, Q_g=12 mC cm^{-2}, **e** Au (111)/Py-LA SAM/PPy: E_g=0.792 V, Q_g=5 mC cm^{-2}, and **f** Au(111)/PPy: E_g=0.792 V, Q_g=5 mC cm^{-2}

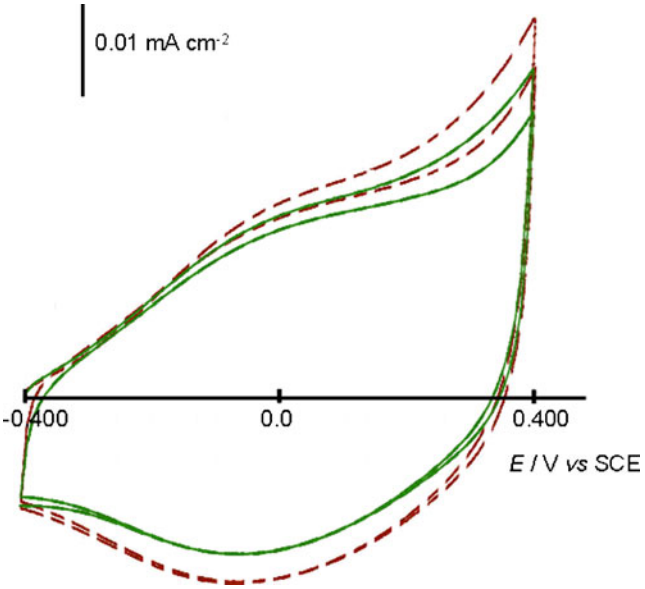

Fig. 9 Cyclic voltammograms of the PPy films potentiodynamic grown at υ=0.05 V s^{-1}on (*dashed line*) Au(111)/PPy with four cycles and (*solid line*) Au(111)/Py-LA SAM/PPy with six cycles, in monomer-free solution

polymer oxidation and reduction process was assumed to be assured just by anions movement [63, 64]; it has been recognized later that protons [65, 66] and other cations [67, 68] may also participate in the process, depending on the size and nature of these species.

Under the conditions employed in the present work, the claimed incorporation of protons into PPy (ClO_4^-) during the electrochemical dedoping process in aqueous solution [65] as well as its subsequent expulsion during doping course cannot be retrieved from the voltammetric data. Indeed the oxidation/reduction current waves are broad enough to cope with the transport of dopant anions, electrolyte cation, protons, and solvent throughout the polymer, but do not allow to discriminate the correspondent fluxes.

In Fig. 9, the dashed and full curves represent the electrochemical behavior of potentiodynamically prepared PPy on Au and on Py-LA SAM; in both cases, the shape and position of the redox conversion are remarkably similar, pointing to no further influence of the SAM apart from to deter the electropolymerization, requiring a higher number of potential cycles in order to observe films with close electroactivity than those deposited on Au (Q_{ox}= 0.49 mC cm^{-2} for PPy generated with six cycles on the SAM modified electrode, whereas four cycles on gold produce a film displaying Q_{ox}=0.54 mC cm^{-2}). As expected, the same applies to the results of the analogous experiments with PPy films grown under potentiodynamic control (Fig. 10). In fact, for growth potential (E_g) of 0.740 V, Fig. 10a, using about the same growth charge (5 mC cm^{-2}) the PPy grown on SAM has smaller electroactivity than that obtained when the film is deposited on Au (Table 1).

The redox conversion of PPy prepared at higher potential values, e.g. 0.792 V, or with different thicknesses is alike. Worth noting that the oxidation charge/reduction charge (Q_{ox}/Q_{red}) ratio (Table 1) is relatively higher for films potentiostatically formed on SAMs, than usually observed for electronically conducting polymers [69] and namely for PPy [53].

In spite of the research reports using scanning probe microscopy on the effect of the doping state on the morphological properties of PPy [70–72], the volume changes associated to PPy redox switching has been subject of some controversy. By in situ STM characterization under

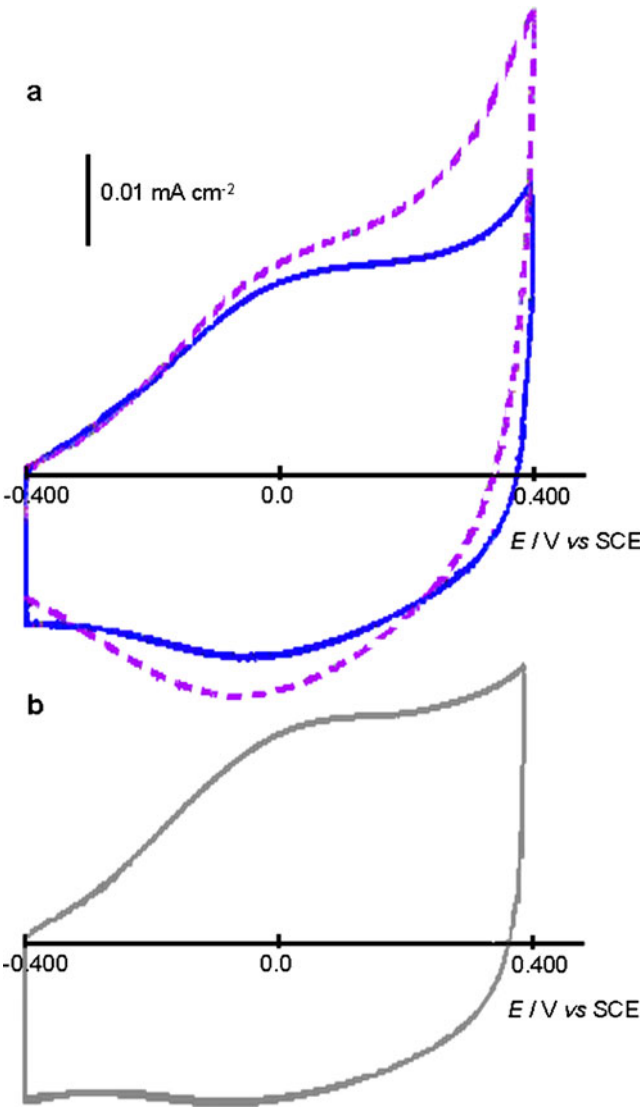

Fig. 10 Cyclic voltammograms of the PPy films potentiostatically grown with Q_g=5 mC cm^{-2} at **a** E_g=0.740 V on Au(111)/PPy (*dashed line*) and Au(111)/Py-LA SAM/PPy (*solid line*) and **b** E_g=0.792 V on Au(111)/Py-LA SAM/PPy, in monomer-free solution

Table 1 Oxidation (Q_{ox}) and reduction charge (Q_{red}) plus Q_{ox}/Q_{red} ratio of the PPy films, synthesized under different electropolymerization conditions and substrates and characterized in 0.1 M $LiClO_4$ at υ=0.05 V/s, E=[−0.400, +0.400]V vs. SCE

Growth mode	Substrate/Film $_{\text{growth charge/mC cm}^{-2}}$	Q_{ox}/mC cm^{-2}	Q_{red}/mC cm^{-2}	Q_{ox}/Q_{red}
Potentiostatic Eg=0.792 V	Au(111)/Py-LA SAM/$PPy_{5.9}$	0.43	0.31	1.39
	Au(111)/Py-LA SAM/$PPy_{8.9}$	0.76	0.64	1.19
	Au(111)/Py-LA SAM/$PPy_{15.5}$	1.05	0.89	1.18
Potentiostatic Eg=0.740 V	Au(111)/Py-LA SAM/$PPy_{5.0}$	0.41	0.34	1.21
	Au(111)/Py-LA SAM/$PPy_{12.1}$	1.19	0.91	1.31
	Au(111)/$PPy_{5.8}$	0.58	0.47	1.23
Potentiodynamic	Au(111)Py-LA SAM/$PPy_{6\ \text{cycles, 50 mV s}^{-1}}$	0.49	0.39	1.26
	Au(111)/PPy4 cycles, 50 mV s^{-1}	0.54	0.43	1.26

potential control it was shown [73] that a swelling of the polymer matrix occurs due to the insertion of counter-ions; on the other hand, an in situ AFM study revealed that throughout the first reduction, a perchlorate-doped PPy, in aqueous solution of $NaClO_4$, undergoes initially rapid swelling and subsequent slow shrinking, with no significant changes in volume during further redox conversions [61]; a reversible expansion of 30% in PPy film thickness upon reduction by scanning the potential has also been claimed [66, 74].

Figure 11 shows in situ AFM images illustrating the morphologies of a thick PPy film (grown with 25 potential cycles on gold modified with Py-LA SAM), in $LiClO_4$ solution, during sequential oxidation and reduction, by stepping the potential from 0.300 to −0.300 V. Remarkable changes are observed, being clear that upon reduction the PPy nodules increase substantially in size and change the shape from globules to a more oval structure. The outcome is similar in subsequent oxidation and reduction scans (Fig. 11a).

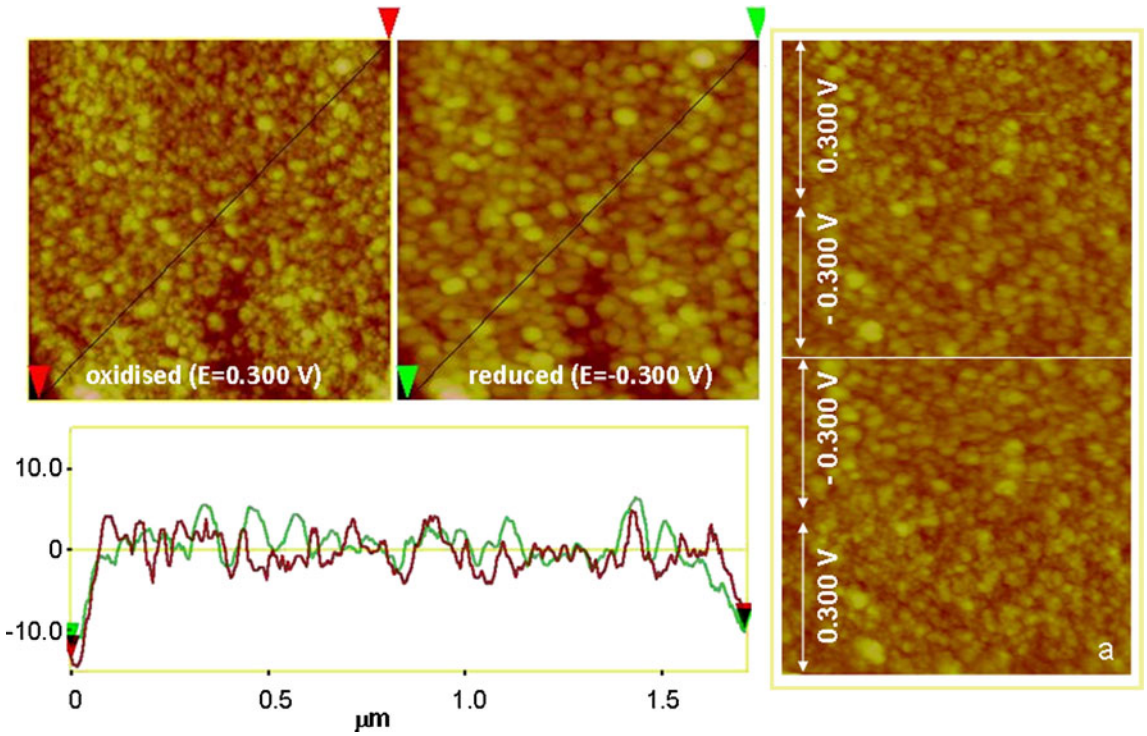

Fig. 11 In situ topographic AFM images of PPy films grown potentiodynamically on Au (111)/Py-LA SAM with 25 polymerization cycles at ν=0.05 Vs^{-1}, in 0.1 M $LiClO_4$. *Left* and *right image* with 1.2× 1.2 µm^2 window size and profile diagram. **a** Images recorded of the Au (111)/Py-LA SAM/PPy (25 cycles) during the negative shift of the substrate potential first from 0.300 to −0.300 V (*top image*) and subsequently during the positive shift of the substrate potential from −0.300 to 0.300 V vs. SCE (*down image*). In all topographic images Z=40 nm

To explain these morphological changes, consistently observed during PPy doping/dedoping process, phase relaxation due to solvent transport through the polymer and inherent structural rearrangement, and ion transport for charge compensation inside the film, must obviously be taken into account. However, even taking for granted the incorporation of protons and solvated Li ions during electrochemical reduction, it is not plausible to consider that the charge compensation is repeatedly accomplished by cation transport rather than anion expulsion from the film (as reported for the very early stages of redox reaction of PPy on gold [61]); still the small size of the inserted cationic species could not dilate the PPy in the extent revealed by Fig. 11. Thus, a significant contribution must arise from the underlying SAM reorganization induced by the applied potential.

Conclusions

Under potentiostatic or potentiodynamic control, the electrochemical deposition of PPy over monolayers of pyrrolyl lipoic acid derivative self-assembled on Au is observed without SAM decomposition or removal. In aqueous solutions of $LiClO_4$, the monomer and monolayer oxidation potentials are about the same but a small blocking action of the SAM is noticed in the polymerization onset, by the later formation of polymer first nuclei (potentiostatic growth) or lower overall current (electropolymerization carried out by cyclic voltammetry) in comparison to the results collected in bare gold. However, polymer film thickening is not significantly affected by the presence of the SAM.

The morphology and structure of PPy films formed on the SAMs were characterized by AFM and XRD, which revealed that those polymer properties are much more influenced by the electrochemical mode of preparation, than by the underlying SAMs. Nevertheless certain changes are worth mentioning. When the electropolymerization is carried out potentiodynamically, the underlying SAM appears to give rise to distinct surface areas, where nodules or relatively long segments are seen by AFM. In the case of the layers deposited at constant potential, the semicrystalline nature of the so-obtained thin PPy layers is not altered by depositing the polymer over the SAM. In contrast, the SAM appears to induce some order on the first layers of the polymer film, as denoted by the modification of the XRD spectrum obtained for PPy on bare gold, i.e. the broad peak, assigned to the PPy amorphous character, suffers a decrease and, concomitantly, two diffraction waves surge.

Thick layers display the typical PPy globular morphology. Their redox behavior, analyzed by in situ AFM, showed a significant increase in volume of the polymer nodules upon reduction. Taking into account the solvent and supporting electrolyte nature, the major part of this outcome is undoubtedly attributable to the reorganization of the underlying SAM induced by the applied potential. Indeed, it also explains the above mentioned features observed for PPy layers deposited by potential cycling.

Acknowledgments The authors thank to J.F. Cabrita for her enthusiasm in carrying out some preliminary experiments.

A. Mourato gratefully acknowledges the financial support by "Fundação para a Ciência e Tecnologia" (SFRH/BPD/35036/2007).

References

1. Wurm DB, Kim YT (2000) Langmuir 16:4533
2. Bartlett PN, Grossel MC, Barrios EM (2000) J Electroanal Chem 487:142
3. Cai X, Jaehne E, Adler HJP (2004) Macromol Symp 210:131
4. Lallemand F, Auguste D, Amato C, Hevesi L, Delhalle J, Mekhalif Z (2007) Electrochim Acta 52:4334
5. Mazur M, Krysinski P (2001) Langmuir 17:7093
6. Huang Z, Wang PC, MacDiarmid AG, Xia Y, Whitesides G (1997) Langmuir 13:6480
7. Smela E (1998) Langmuir 14:2996
8. Rozsnyai LF, Wrighton MS (1994) J Am Chem Soc 116:309
9. Liu G, Böcking T, Gooding JJ (2007) J Electroanal Chem 600:335
10. Kim YH, Wurm DB, Kim MW, Kim YT (1999) Thin Solid Films 352:138
11. Willcut RJ, McCarley RL (1995) Adv Mater 7:759
12. Bernard MC, Chausse A, Cabet-Deliry E, Chehimi MM, Pinson J, Podvorica F, Vautrin C (2003) Chem Mater 15:3450
13. Stewart MP, Maya F, Kosynkin DV, Dirk SM, Stapleton JJ, McGuiness CL, Allara DL, Tour JM (2004) J Am Chem Soc 126:370
14. Ruckenstein E, Li ZF (2005) Adv Colloidal Interface Sci 113:43
15. Wu CG, Yeh YR, Chen JY, Chiou YH (2001) Polymer 42:2877
16. Wu CG, Hsiao HT, Yeh YR (2001) J Mater Chem 11:2287
17. Ulman A (1996) Chem Rev 96:1533
18. Silva RC, Nicho ME, Resendiz MC, Agarwal V, Castillon FF, Farias MH (2008) Thin Solid Films 516:4793
19. Kline RJ, McGehee MD (2006) J Macromol Sci Part C: Polym Rev 46:27
20. Kline RJ, McGehee MD, Toney MF (2006) Nat Mater 5:222
21. Ong BS, Liu YWP, Gardnes S (2004) J Am Chem Soc 126:3378
22. Wu Y, Liu P, Ong BS, Srikumar T, Zhao N, Botton G, Zhu S (2005) Appl Phys Lett 86:142102
23. Sutar DS, Padma N, Aswal DK, Deshpande SK, Gupta SK, Yakhmi JV (2007) J Colloid Interface Sci 313:353
24. Bain CD, Troughton EB, Tao Y, Evall TJ, Whitesides GM, Nuzzo RG (1989) J Am Chem Soc 111:321
25. Lukkari J, Kleemola K, Meretoja M, Ollonqvist T, Kankare J (1998) Langmuir 14:1705
26. Hayes WA, Shannon C (1996) Langmuir 12:3688
27. Love C, Estroff L, Kriebel KJ, Nuzzo GR, Whitesides GM (2005) Chem Rev 105:1103
28. Sayer CN, Collard DM (1995) Langmuir 11:302
29. Shustak G, Domb AJ, Mandler D (2006) Langmuir 22:5237
30. Vercelli B, Zotti G, Berlin A, Grimoldi S (2006) Chem Mater 18:3754
31. Wurm DB, Brittain ST, Kim YT (1996) Langmuir 12:3756
32. McCarley RL, Willcut RJ (1998) J Am Chem Soc 120:9297
33. Hasegawa S, Horigome T, Yakushi K, Inokuchi H, Okudaira-Kamiya K, Ueno N, Seki K, Willicut RJ, McCarley RL,

Morikawa EE, Saile V (2001) J Electro Spectrosc Relat Phen 113:101
34. Wu CG, Chiang SC, Wu CH (2002) Langmuir 18:7473
35. Li XM, Husken JS, Reinhoudt DN (2004) J Mater Chem 14:2954
36. Fabre B, Ababou-Girard S, Solal F (2005) J Mater Chem 15:2575
37. Shen Y, Gong S, Zhou W, Li J (2005) Colloids Surf A: Physicochem Eng Aspects 257:149
38. Willcut RJ, McCarley RL (1994) J Am Chem Soc 116:10823
39. Collard DM, Sayer CN (1995) Synth Met 69:459
40. Willcut RJ, McCarley RL (1995) Langmuir 11:296
41. Willcut RJ, McCarley RL (1995) Anal Chim Acta 307:269
42. Collard DM, Sayer CN (1997) Synth Met 84:329
43. Grace AN, Pandian K (2003) J Solid State Electrochem 7:296
44. Intelmann CM, Rammelt U, Plieth W, Cai X, Jähne E, Adler H-P (2006) J Solid State Electrochem 11:1
45. Michalitsch R, El KA, Yassar A, Lang P, Garnier F (1998) J Electroanal Chem 457:129
46. Inaoka S, Collard DM (1999) Langmuir 15:3752
47. Sato N, Nonaka T (1995) Chem Lett 24:805
48. Berlin A, Zotti G (2000) Macromol Rapid Commun 21:301
49. Cabrita JF, Viana AS, Eberle C, Montforts FP, Mourato A, Abrantes LM (2009) Surf Sci 603:2458
50. Widrig CA, Chung C, Porter MD (1991) J Electroanal Chem 310:335
51. Daniel MC, Astruc D (2004) Chem Rev 104:293
52. Chidsey CED, Liu GY, Powntree P, Scoles G (1989) J Chem Phys 91:4421
53. Mesquita JC (1993) Ph.D. thesis, University of Lisbon
54. Cheah K, Forsyth M, Truong VT (1998) Synth Met 94:215
55. Hussian AMP, Saikia D, Singh F, Avasti DK, Kumar A (2005) Nucl Instrum Methods Phys Res B 240:834
56. Warren MR, Madden JD (2006) Synth Met 156:724
57. Geng W, Li N, Li X, Wang R, Tu J, Zhang T (2007) Sens Actuactors B 125:114
58. Dureklev P, Granström M, Inganas O, Gunaratne LMWK, Senadeera GKR, Skaarup S, West K (1996) Polymer 37:2609
59. Ashrafi A, Golozar MA, Mallakpour S (2006) Synth Met 156:1280
60. Boubour E, Lennox RB (2000) Langmuir 16:7464
61. Suárez MF, Compton RG (1999) J Electroanal Chem 462:221
62. Tourillon G, Dartyge E, Fontaine A, Garrett R, Sagurton M, Xu P, Williams G (1987) Europhys Lett 4:1391
63. Diaz AF, Kanazawa KKJ (1979) J Chem Soc Chem Commun 635
64. Diaz AF (1981) Chem Scripta 17:145
65. Tsai EW, Jang G, Rajeshwar K (1987) J Chem Soc Chem Commun 1776
66. Christensen PA, Hamnett A (1991) Electrochim Acta 36:1263
67. Inganäs PQ (1992) J Phys Chem 96:10507
68. Arca M, Mirkin MV, Bard A (1995) J Phys Chem 99:5040
69. Rodriguez J, Grande HJ, Otero TF (1997) In: Nalwa HS (ed) Handbook of organic conductive molecules and polymers. Chichester, Wiley, p 452
70. Li J, Wang E, Green M (1995) Synth Met 74:127
71. Silk T, Hong Q, Tamm J, Compton R (1998) Synth Met 93:59
72. Silk T, Hong Q, Tamm J, Compton R (1998) Synth Met 93:65
73. Chaînet E, Billon M (1998) J Electroanal Chem 451:273
74. Hamnett A, Christensen PA, Higgins S (1994) Analyst 119:735
75. Rajendran S, Prabhu MR, Rani MU (2008) Int J Electrochem Sci 3:282